Ocean Sci., 6, 219–234, 2010
www.ocean-sci.net/6/219/2010/

Ocean Science

Heat in the Barents Sea: transport, storage, and surface fluxes

L. H. Smedsrud[1], **R. Ingvaldsen**[2,1], **J. E. Ø. Nilsen**[3,1], **and Ø. Skagseth**[2,1]

[1]Bjerknes Centre for Climate Research, Bergen, Norway
[2]Institute of Marine Research, Bergen, Norway
[3]Nansen Environmental and Remote Sensing Centre, Bergen, Norway

Received: 25 June 2009 – Published in Ocean Sci. Discuss.: 7 July 2009
Revised: 25 January 2010 – Accepted: 2 February 2010 – Published: 11 February 2010

Abstract. A column model is set up for the Barents Sea to explore sensitivity of surface fluxes and heat storage from varying ocean heat transport. Mean monthly ocean transport and atmospheric forcing are synthesised and force the simulations. Results show that by using updated ocean transports of heat and freshwater the vertical mean hydrographic seasonal cycle can be reproduced fairly well.

Our results indicate that the ∼70 TW of heat transported to the Barents Sea by ocean currents is lost in the southern Barents Sea as latent, sensible, and long wave radiation, each contributing 23–39 TW to the total heat loss. Solar radiation adds 26 TW in the south, as there is no significant ice production.

The northern Barents Sea receives little ocean heat transport. This leads to a mixed layer at the freezing point during winter and significant ice production. There is little net surface heat loss annually in the north. The balance is achieved by a heat loss through long wave radiation all year, removing most of the summer solar heating.

During the last decade the Barents Sea has experienced an atmospheric warming and an increased ocean heat transport. The Barents Sea responds to such large changes by adjusting temperature and heat loss. Decreasing the ocean heat transport below 50 TW starts a transition towards Arctic conditions. The heat loss in the Barents Sea depend on the effective area for cooling, and an increased heat transport leads to a spreading of warm water further north.

1 Introduction

Despite being shallow and small, the Barents Sea is special because it dominates Arctic Ocean heat storage (Serreze et al., 2007). With a mean depth of 230 m, and an area ∼14% of the Arctic Ocean, more than 50% of the Arctic Ocean winter heat loss occur in the Barents Sea (Serreze et al., 2007). This happens because the relatively large open water areas in the Barents Sea allow both large absorption of incoming solar radiation during spring and summer, and stronger heat loss in autumn and winter than the other Arctic Seas.

When other Arctic Seas freeze over and are insulated from further cooling by sea ice, the southern Barents Sea remains open, and is convectively cooled for the major part of the water column. In this way most of the ocean heat is lost every winter, and the Barents Sea remains open and coupled to the atmosphere. If this heat was not re-supplied by the ocean transport, the Barents Sea surface would drift towards the freezing point after a few years, as will be demonstrated in this paper. Figure 1 shows the major ocean transport into, and out of, the Barents Sea as it will be presented here.

Several numerical models have been applied to the Barents Sea suggesting strong year to year variability (Zhang and Zhang, 2001; Gerdes et al.,2003; Harms et al., 2005; Budgell, 2005; Maslowski et al., 2004). Two new model studies addressing the Barents Sea variability are also completed, Årthun and Schrum (2010) discuss the long term variability since 1950, and Sandø et al. (2010) the shorter term lead and lag correlations. We aim to take an integrated model approach and establish a mean over the Barents Sea. By doing this we do not describe the gradual transformations, and any internal variability, but this has been discussed and described by the applied 3-D models above. Harms et al. (2005) concluded that there are large uncertainties in the forcing applied, but also that there is a clear dominance of the Barents Sea inflow on the variability.

Correspondence to: L. H. Smedsrud
(lars.smedsrud@uni.no)

Published by Copernicus Publications on behalf of the European Geosciences Union.

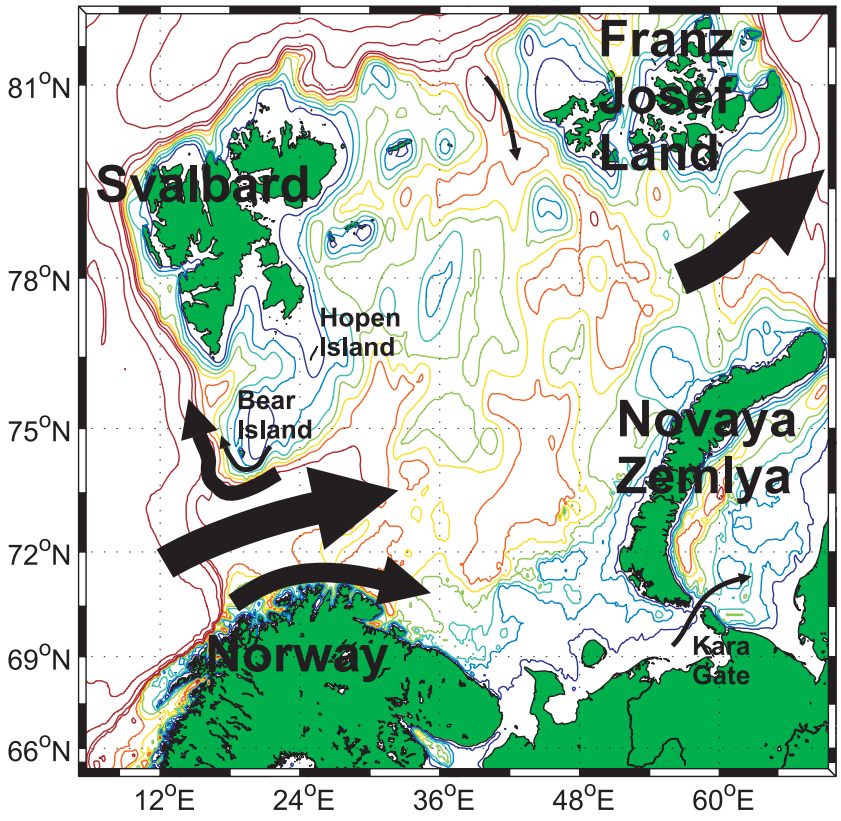

Fig. 1. The Barents Sea and surrounding islands. Mean flow is sketched based on various sources described in the text (arrow width is scaled using 0.1 Sv=1.0 pt). Depth contours are plotted for 50 m, 100 m, 150 m, 200 m, 250 m, 300 m, 400 m, 500 m, 1000 m, and 2000 m.

In this paper we use existing transport estimates, based on observations and the 3-D models, to find a relation between the heat transported into the sea, and the heat fluxes at the surface. We will evaluate this relation, between the ocean heat transport and the vertical heat fluxes, towards the mean temperature field using a vertical column model. The main advantage of using a simple column model is that it can be evaluated towards all available profiles averaged into one horizontal mean. Additionally forcing and boundary conditions can be directly based on observations. The column model approach also has clear limitations, any internal horizontal gradients are not represented, and values found are averages over a large horizontal area. The term "ocean heat transport" will be used consistently for the heat carried by the ocean currents. The term "heat flux" will be used for vertical exchange, i.e. air-sea-ice fluxes at the surface.

An updated synthesis of the mean state of the Barents Sea is given in Sect. 2, including transport of heat and freshwater. Based on published values we first define a best estimate closed volume budget for the Barents Sea, a prerequisite to consistent heat and freshwater budgets (Montgomery, 1974; Schauer et al., 2008). These budgets are then used in Section 3 in combination with surface flux data as forcing to the model, to evaluate if these represent realistic and balanced sets of forcing fields. This is done by comparing the modeled and observed mean hydrographic seasonal cycle of the Barents Sea. To establish a realistic set of forcing fields is the basis for Sect. 4 dealing with the sensitivity test of the Barents Sea to possible changes in the forcing.

2 Barents Sea mean state

Ocean transport has a strong influence on the Barents Sea mean state (Mosby, 1962). The warm water entering in the main inflow area, the Barents Sea Opening (BSO) becomes gradually cooled and freshened before it exits the Barents Sea (Fig. 1). Figure 2 shows that winter surface temperatures in the BSO reaches 5 °C (Nilsen et al., 2008). The 0 °C isotherm extend almost to the southern tip of Novaya Zemlya. During summer the 6 °C isotherm almost reaches the southern tip of Novaya Zemlya, and the maximum temperatures in the BSO are 8–9 °C (not shown). This means that the gross southern Barents Sea temperature gradient is similar all year, but stronger in winter than summer.

In contrast to the south, the northern Barents Sea is normally ice covered during winter. The surface layer in the north is thus close to freezing during winter (Fig. 2), increasing to 0–2 °C during summer. Below the surface layer the mean salinity in the southern parts carries the influence of

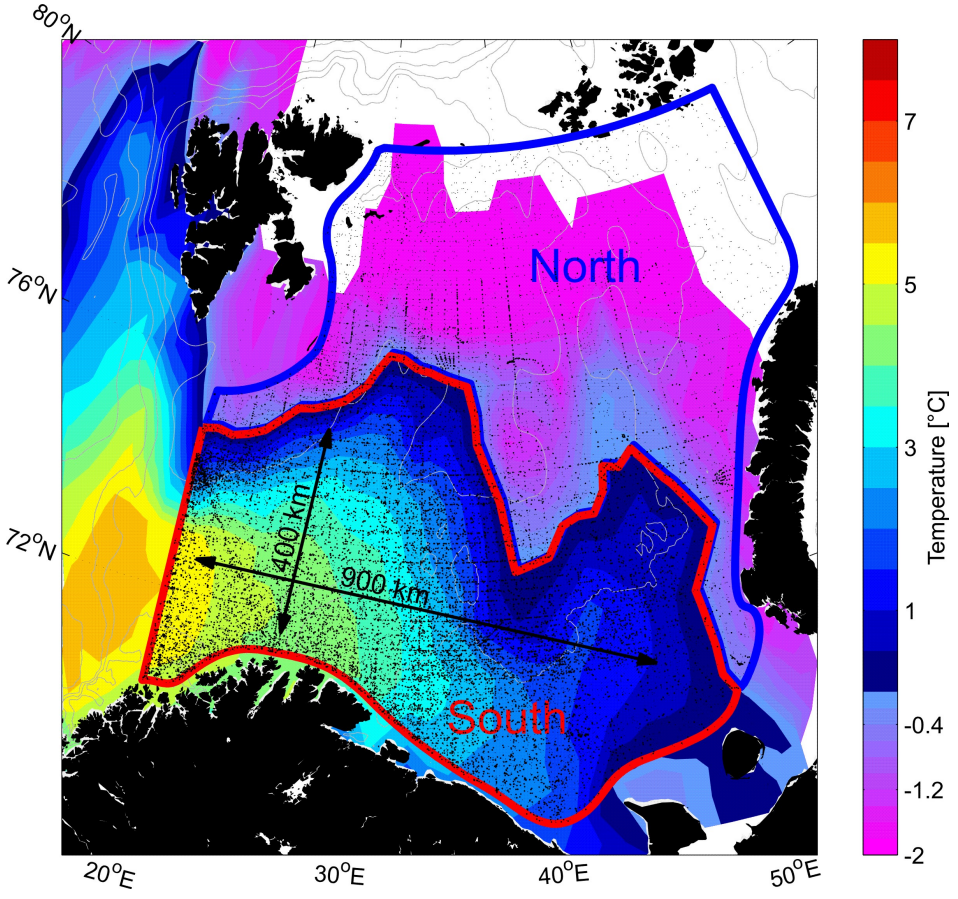

Fig. 2. Mean temperature during winter at 10 m depth (Albers Equal-Area Conic map projection, data from Nilsen et al., 2008). Positions of the 55 000 stations used is shown with black dots. The Barents Sea is divided into two boxes; "North" and "South" defined by the mean winter 0 °C surface isotherm.

Atlantic Water inflow with a salinity around 35.1. The mean salinity of the Atlantic inflow is discussed in Sect. 2.3. Surface salinities generally decrease towards the southeastern coast and the surrounding islands, reflecting freshwater input from land (Sect. 2.3), and towards the northern parts due to ice melting. The Barents Sea variability is substantial from year to year, and some of this variability will be described in the sections below.

2.1 Barents Sea volume budget

The net flow through the BSO based on observations is 2.0 Sv eastwards (1 Sv=1×10^6 m^3/s). This net flow is derived from four sources; the inflowing Norwegian Coastal Current (NCC) at the southern coast, the Atlantic inflow in the central area, and two westward flows in the northern areas (Fig. 1).

The contribution from the NCC is 1.2 Sv. This estimate is based on current meter and hydrography data in Skagseth et al. (2010). In the center of the BSO is the Atlantic inflow that has been monitored by an array of current meters since 1997 in addition to standard hydrographic sections (Ingvaldsen et al., 2004; Skagseth et al., 2008). New data included here complements this series up to 2007, and the 1997–2007 mean inflow is 2.0 Sv. Finally, 0.9 Sv leaves in the Bear Island Trench (Skagseth, 2008), and another ∼0.3 Sv in the shallow Bear Island Current (Blindheim, 1989). Thus, there is an inflow of 3.2 Sv and an outflow of 1.2 Sv giving a net eastward flow of 2.0 Sv.

Several different ocean models run with reanalysis forcing show mean net flux in the BSO in accordance with the results presented here, although the inflow and outflow in the models differ substantially (e.g. Drange et al., 2005; Aksenov et al., 2010). A longer term trend in the BSO is not clearly seen from numerical model studies, as both no trend (Gerdes et al., 2003) and a positive significant trend (Årthun and Schrum, 2010), has been found.

Inflow of Atlantic Water in the BSO is higher during winter related to the stronger winds (Ingvaldsen et al., 2004). An annual mean cycle based on 1997–2007 data shows a January maximum of 2.8 Sv, falling to an April minimum of 1.3 Sv. The rest of the year it is close to the mean of 2.0 Sv (Table 1).

Table 1. Monthly means for each calender month over the Barents Sea area. Atlantic inflow is updated from Ingvaldsen et al. (2004) and Skagseth et al. (2008) setting the monthly varying transport. The other data included are based on existing estimates cited in the text.

Parameter	Jan	Feb	Mar	Apr	May	Jun	Jul	Aug	Sep	Oct	Nov	Dec	Mean
Solar radiation W m^{-2}	0.0	1.8	33.7	106.2	183.4	227.4	203.3	133.9	55.2	9.4	0.1	0.0	79.5
Long wave in W m^{-2}	224.3	226.9	232.7	239.4	267.4	286.4	299.0	293.5	281.1	258.6	239.0	227.9	256.4
Air temp. °C	−11.6	−12.2	−9.8	−8.6	−2.6	1.6	3.5	3.9	2.5	−2.4	−6.8	−10.0	−4.4
Relative humidity %	80	81	81	80	81	87	91	88	85	80	81	80	84
Snow fall mm/month	11.1	9.9	7.8	6.6	3.9	1.2	0.0	0.0	1.5	7.2	8.7	11.1	5.8
Snow albedo	0.85	0.84	0.83	0.81	0.82	0.78	0.64	0.69	0.84	0.85	0.85	0.85	0.80
Mean wind m/s	9.3	9.2	8.7	7.4	6.1	5.8	5.2	5.7	6.7	7.6	8.6	9.0	7.4
Wind std deviation m/s	4.7	4.7	4.2	3.8	3.4	3.2	2.9	3.2	3.6	4.1	4.3	4.3	3.9
Atlantic volume transport (Sv)	2.8	2.3	2.1	1.3	1.7	1.9	1.7	2.1	1.8	1.8	2.2	1.9	2.0
Varying volume transport (Sv)	+0.8	+0.3	+0.1	−0.7	−0.3	−0.1	−0.3	0.1	−0.2	−0.2	+0.2	−0.1	0

The main outflow of ∼2.0 Sv from the Barents Sea takes place between Novaya Zemlya and Frans Josef Land (Gammelsrød et al., 2009), termed the Barents Sea eXit (BSX, Fig. 1). The annual cycle is similar to that in the BSO, with the largest outflow during winter above 2.0 Sv (Schauer et al., 2002). Long term model results by Gerdes et al. (2003) state a 1948–2002 variability in the BSX between 1.0 and 2.6 Sv, with a mean around 1.5 Sv.

In addition to the major inflow in the BSO and the outflow in the BSX there is 0.3 Sv leaving through the Kara Gate between Novaya Zemlya and the Russian coast (Karcher et al., 2003; Maslowski et al., 2004). This outflow is approximatedly balanced by the 0.3 Sv entering in the north between Svalbard and Franz Josef Land (Maslowski et al., 2004).

The volume budget used as model forcing is a mean inflow and outflow of 3.2 Sv for the southern Barents Sea, and 2.0 Sv for the northern Barents Sea (Fig. 1). We use a fixed annual cycle from the well sampled Atlantic inflow around these means (Table 1). This is a simplified, but closed, volume transport budget, that will serve as a basis for the ocean transport of heat and salt discussed below. We note that the Atlantic inflow contributes with 63%, and is thus dominating, but the remaining 37% cannot be ignored. The closed volume budget enables correct calculations of heat transport, in line with Montgomery (1974), to the horizontally averaged Barents Sea area used by the model.

A few more contributions have been estimated, but values are small enough to ignore them in the overall volume budget. This includes input from rivers, rain and sea ice transport, amounting to ∼0.04 Sv. These contributions are significant in the Freshwater budget and are discussed in Sect. 2.3. This freshwater input is similar in magnitude to the outflow of dense water produced in the largest fjord around Svalbard (Storfjorden). Inflow of Atlantic Water also occurs here, but this water re-circulate south of Svalbard (O'Dwyer et al., 2001). Due to two shallow banks (<100 m depth, Bear Island and Hopen banks) with steep topography south of Svalbard, this part of the Barents Sea has limited exchange of water with the rest of the sea. This area is therefore also excluded from the "North" area in Fig. 2.

2.2 Heat transport

It was early recognized that the Barents Sea climate is largely controlled by ocean heat transport (Mosby, 1962). Strong correlations between inflow and temperature and the large-scale atmospheric pattern upstream in the Norwegian Sea (the North Atlantic Oscillation) have also been well documented (Loeng et al., 1997; Dickson et al., 2000; Furevik, 2001). Low temperature anomalies in the BSO during the 1980's are also paralleled by low salinity anomalies (Blindheim, 1989; Dickson et al., 2007).

Heat transport will be referenced to 0 °C which is close to the outflow temperature in the BSX (Schauer et al., 2002). Having a closed volume budget (Sect. 2.1) the choice of reference temperature is arbitrary for the heat transport estimates as long as the reference temperature is the same for both inflow and outflow. In this study we generally present heat transports and fluxes using TW (1 TW=1×10^{12} W), but individual vertical heat fluxes at the surface will sometimes be discussed in W/m^2.

The 1997–2007 mean heat transport by the Atlantic Water in the Barents Sea Opening is 49.7 TW (Skagseth et al., 2008). This heat transport compares to cooling the inflowing 2.0 Sv from 6.1 °C to 0 °C. Changes in the heat transport may be equally caused by changes in the inflow and outflow temperatures, or changes in the volume transport. The de-seasoned inflow temperature spans a range from ∼4.3 °C to ∼6.4 °C and has increased from ∼5 °C in the 1960's to ∼6 °C after 2000 (Skagseth et al., 2008). Transport of heat has been high in recent years, and the yearly mean heat transport has since 2002 been above 50 TW except for 2004. During the last 10 years, variation in ocean volume flux is the main cause for variation in ocean heat transport (Skagseth et al., 2008). The lowest heat transport was measured in 2001 at 30 TW, and corresponded to a relatively low annual mean inflow close to 1.0 Sv (not shown).

Figure 3 shows the mean annual cycle of heat transport compared to an estimate from using a monthly varying volume transport and a constant inflow temperature of 6.1 °C. Compared to the calculated heat flux using the individual

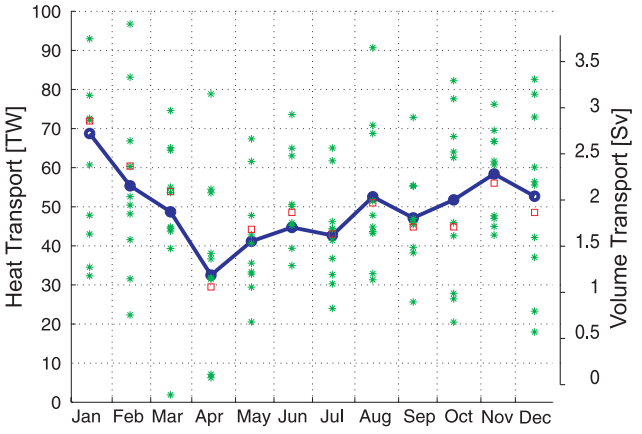

Fig. 3. Atlantic heat transport through the Barents Sea Opening. Blue solid line shows the overall annual mean cycle of heat transport referenced to 0 °C for the 1997–2007 data. Green asterisks show individual monthly heat transport. The corresponding cycle of volume transport (Table 1) is plotted as red squares in relation to the right vertical axis, which scaling corresponds to heat transport calculated from volume transports using a constant inflow temperature of 6.1 °C and outflow at 0 °C.

temperature measurements on each current meter, deviations are generally small, but largest in October at 7 TW. Temperature variations decrease the incoming heat slightly in winter and increase heat flux in summer as one might expect.

The NCC inflow of 1.2 Sv has a likely significant but so far not well quantified contribution. Based on data from a recent one-year full depth current meter profile in the core of the NCC, combined with repeated hydrographic profiles the heat transport of the NCC is estimated to 34 TW (Skagseth et al., 2010). The NCC thus contributes about 1/3 of the ocean heat transport. The coastal current has been included in freshwater budgets for the Barents Sea earlier (Dickson et al., 2007), but the carried heat has so far to a large extent been unknown. Details on the method for estimated NCC volume, heat, and freshwater content are described in Skagseth et al. (2010).

The BSX observations from 1991–1992 indicate a heat transport from the Arctic Ocean to the Barents Sea of ∼4 TW (Gammelsrød et al., 2009). The similar heat transport from Budgell (2005) is 5.6 TW, but from Maslowski et al. (2004) it is −7.4 TW, i.e. a heat loss from the Barents Sea. Model results by Gerdes et al. (2003) produced a 1948–2002 net heat transport to the Barents Sea of ∼7 TW (mean outflow temperature of −0.2 °C), and Aksenov et al. (2010) a 1989–2004 heat transport of ∼4 TW (mean outflow temperature of −0.9 °C). Although the uncertainties are large, we summarise this to a net volume flux here of 2.0±0.6 Sv with a mean temperature close to 0 °C.

The northern inflow of 0.3 Sv (between Svalbard and Franz Josef Land) probably carries less than 1 TW (Aksenov et al., 2010). This is also true for the 0.3 Sv leaving in the Kara Gate (Maslowski et al., 2004). The small 0.3 Sv Bear Island Current (Blindheim, 1989) is also assumed not to transport significant heat, as temperatures are close to zero. The 0.9 Sv leaving in the Bear Island Trench (Skagseth, 2008) does, on the contrary, carry about 12 TW.

In light of the above stated uncertainties some other small heat contributions may be ignored. There is, for example, a contribution from sea ice import from the Arctic estimated to 477 km^2/day (Pavlov et al., 2004), contributing with a heat loss around 1.3 TW, assuming a mean ice thickness of 1 m. In total, the Barents Sea receives 86 TW from the Atlantic inflow and the Norwegian Coastal Current, and looses about 12 TW in the Bear Island Trench, resulting in a net inflow of 73 TW of heat.

The standard model ocean heat transport used is an annual mean of 73 TW, with a monthly variation driven by the volume transport in Table 1. If this transported heat was to be lost from the surface evenly over the Barents Sea area (1.1×10^{12}m^2), a constant net surface heat loss of 66 W/m^2 would be required. A number of sensitivity runs are performed in Sect. 4.1 that span the observed variation in heat transport.

2.3 Freshwater budget

In contrast to the heat budget where the inflow is the major contributor, the freshwater budget is more complicated. The Barents Sea lies between the Nordic Seas and the Arctic Ocean, making the Barents Sea freshwater fluxes relevant for both (Serreze et al., 2006; Dickson et al., 2007). Fluxes of freshwater will be given in mSv (1 mSv=10^3 m^3/s=31.5 km^3/year). The relative contribution of the different freshwater sources is independent of a reference salinity, but we will use a reference salinity of 35.0. This is the middle value between 34.8, used for the Arctic Ocean (Aagaard and Carmack, 1989), and the inflow salinity of 35.2 across the Greenland-Scotland ridge (Dickson et al., 2007). The Barents Sea surface layer is often fresher than 34.8, but at depth salinities approach 35.0.

The Barents Sea receives significant freshwater input from precipitation and rivers. The net Precipitation-Evaporation balance is roughly ∼0.9 mm/day (Walsh et al., 1998), making the freshwater flux $F_{p-e} = 11.45$ mSv, using a Barents Sea area of 1.1×10^{12} m^2. River inflow is larger, and estimated to 632 km^3/year (Dankers and Middelkoop, 2008), equivalent to $F_{\text{river}} \sim 20$ mSv. These two major contributions are pure freshwater ($S = 0$), and thus independent of any choice of reference salinity.

The major balance of the freshwater budget is between the incoming freshwater at the surface, and the removal of freshwater by transport. Following Aagaard and Carmack (1989) and Serreze et al. (2006) a freshwater flux F is based on a volume flux of water V with a salinity S:

$$F = \frac{S_{\text{ref}} - S}{S_{\text{ref}}} \cdot V, \quad (1)$$

and we use $S_{\text{ref}} = 35.0$ as stated in the introduction. The NCC has a mean salinity of 34.34 and $V = 1.2$ Sv, based on the new current meter and hydrographic data (Skagseth et al., 2010). This produces a freshwater flux of F_{NCC}=22.7 mSv, increased significantly from the older estimate of 17.1 mSv based on Blindheim (1989).

Another freshwater source is sea ice import from the Kara Sea and the Arctic Ocean of 477 km^2/day (Pavlov et al., 2004). This converts to a volume transport of V=5.5 mSv assuming 1 m thick ice. Using a sea ice salinity of S=5, we get $F_{\text{sea ice}}$=4.6 mSv. Zhang and Zhang (2001) model results indicate a larger sea ice volume flux (339 km^3/year) translating into ∼10 mSv of freshwater. They also include a significant loss (about 30%) south of Svalbard to the Fram Strait. In their study Zhang and Zhang (2001) found a net precipitation and river runoff much smaller than the ones we have found above, so their net surface freshening is smaller despite the large sea ice contribution.

The total freshwater flux to the Barents Sea is thus of the order 55–60 mSv. How is this freshwater removed? Some of it is compensated by the Atlantic inflow. The Atlantic inflow of 2.0 Sv and the higher than mean salinity $S \sim= 35.1$ (Skagseth, 2008) is counter acting the freshwater input with $F_{\text{Atlantic}} = -5.7$ mSv. But this is only ∼10% of what is needed to balance the input. The outflow contribution in the BSX is larger with $F_{\text{BSX}} = -14.3$ mSv based on 2.0 Sv and $S = 34.75$ water (Gammelsrød et al., 2009). The return flow in the Bear Island Trench does not contribute when using $S_{\text{ref}} = 35.0$ as it has exactly this salinity (Skagseth, 2008). The freshwater input is large compared to the removal of freshwater driven by the through-flow. The relative contributions of these sources and sinks would change if we used a different S_{ref}, but we would still need about 39 mSv of freshwater to be removed from the Barents Sea.

Most of the excess 39 mSv of freshwater probably leaves with the 0.3 Sv exiting through the Kara Gate. A balance may be reached by assuming a mean salinity there of $S = 31.2$. The exchange between Svalbard and Franz Josef Land is then assumed to be balanced in freshwater transport. This implies that the 0.3 Sv entering between Svalbard and Franz Josef Land has a salinity close to 35.0, and that the 0.3 Sv in the Bear Island Current has a salinity of 34.75.

A rough balance can thus be achieved between the freshwater associated with through-flow of Atlantic Water ($F_{\text{Atlantic}} + F_{\text{BSX}} = -20$ mSv), the freshwater from precipitation-evaporation, the sea ice, and ∼18% of the NCC. This freshwater redistribution is used as forcing in the model as described in Sect. 3.1. The forcing adds freshwater homogeneously above 60 m, and removes the same amount of freshwater homogeneously below 60 m depth. All the river water remains along the coast, and exit through the Kara Gate. Of the freshwater in the NCC 55% also remains along the coast and exit in the Kara Gate, the remaining 27% exits as the fresh surface Bear Island Current. The freshwater along the coast, and that exiting in the surface, is not accounted for in the model as it enters and exits at the same depth.

3 Barents Sea column modelling

The 1DICE column model is forced by monthly mean observations and calculates the horizontally averaged ice thickness and the ocean column below. 1DICE was developed and described by Björk (1989, 1997). A version of 1DICE with an active atmosphere, fluxes from rivers and the Bering Strait, as well as ice export, was applied in Björk and Söderkvist (2002). A simpler setup of 1DICE is used here; a 1 m vertical resolution is used down to a representative Barents Sea depth, the atmosphere is purely external forcing. The mean depth of the southern Barents Sea is 253 m, the northern column is 210 m deep.

In the model, a stable annual cycle is usually established within 3 years, and model runs were therefore performed over 10 years with a daily time step. The model mixed layer has instant mixing, and the diffusivity below the mixed layer is constant, normally set to $K_z = 5.0 \times 10^{-6}$m^2/s. As the Barents Sea in many model runs enters a state of convection to the ocean floor during winter, diffusion plays a role mostly during summer, mixing the warmer mixed layer downwards.

Radiative fluxes are key controlling factors all over the Arctic. As argued by Eisenman et al. (2007) many models use the albedo as a "tuning parameter" to correctly model the ice cover. 1DICE is, like any ice-ocean model, sensitive to changes in albedo. A simple thickness dependant bare ice albedo increasing from 0.2 to 0.6 at 2.0 m thickness (Björk and Söderkvist, 2002) is used. One sea ice class is used, meaning that the first year sea ice has the same overall thickness during winter. Few observations of Barents sea ice thickness are available, and no attempt has been made to apply ridging processes or an ice thickness distribution. A more detailed model description may be found in Björk (1997).

The 1DICE calculates surface fluxes based on standard bulk formulas, sea surface temperatures, and the forcing discussed in the next section. Long wave outgoing radiation, latent heat of evaporation, and sensible heat flux are all significant to the total heat loss. 1DICE grows ice and mixes heat and salt/freshwater downwards.

3.1 Model forcing

In addition to the forcing from the ocean transport, 1DICE needs atmospheric forcing. This is incoming radiation (shortwave and long wave), air temperature and humidity, mean winds, and snowfall. The monthly mean forcing used is given in Table 1 and discussed below. The forcing used are horizontally averaged values from the area 12–55° E and 70–80° N, covering the entire Barents Sea. The averaging masks significant gradients in the horizontal forcing fields, but the sensitivity towards this forcing is addressed separately. Data

from ECMWF (ERA 40) and NCAR-NCEP reanalyses have been compared to data from the International Satellite Cloud Climatology Project (version 1, the polar ISCCP, and version 2 the Surface Radiation Budget, SRB).

Surface solar radiation peaks at 227 W/m^2 in June for the satellite derived data and ERA 40, whereas NCEP has an additional 100 W/m^2. We have chosen to use the mean of the SRB and Polar ISCCP data. The ERA 40 is almost identical to the Satellite data, but April–May solar radiation is $\sim$10 W/m^2 higher, while July–August is $\sim$20 W/m^2 lower. November through February is identical for the different sources.

Long wave incoming radiation is high all year, but also peaks in summer. We use the SRB fluxes as they are close to the mean based on all the sources. NCEP is $\sim$20 W/m^2 lower all year, while ERA 40 is $\sim$20 W/m^2 higher in summer, and ISCCP is $\sim$20 W/m^2 higher in winter.

The satellite sources do not have air temperature, so the values in Table 1 are means based on ERA 40 and NCEP. ERA 40 is warmer during summer, and NCEP is warmer during winter. The Barents Sea surface air temperatures gets as low as $-12.2\,^\circ$C in February, and as high as $+3.9\,^\circ$C in August. The means used are close to the mean air temperature from the meteorological stations in the southern Barents Sea; at Bear Island, Hopen Island, Murmansk and southern Novaya Zemlya during winter (1961–1990 normals, http://eklima.met.no and http://www.ncep.noaa.gov). During summer (June–August), the meteorological stations have 2–3 °C higher air temperatures. Thus, the reanalysis fields give reasonable estimates, at least in the southern Barents Sea.

The air temperature decrease strongly northwards in the Barents Sea. Two meteorological stations in the northern parts (Victoria Island and Franz Josef Land), are in general 10–12 °C colder than the mean based on ERA40 and NCEP during winter, and 3–4 °C colder during summer (1961–1990 normals, http://eklima.met.no). The effect of changes in air temperature are examined in sensitivity runs, using both a warmer and colder atmosphere.

Relative humidity of the atmospheric boundary layer is high throughout the year, as one would expect over an ocean. Values increase during summer both for NCEP and ERA 40 from a constant level in winter close to 80%. We use the mean of the two reanalyses, producing the annual mean of 84%.

Snow fall is applied as direct forcing (Table 1), and melts due to surface heat fluxes. Rain is accounted for through the freshwater budget discussed earlier (Sect. 2.3). The ERA 40 data used here indicates $\sim$10 mm/month during winter. Total precipitation from the two met stations indicate a larger precipitation of 31 mm/month for Bear Island and 40 mm/month for Hopen Island (1961–1990 normals, http://eklima.met.no). Such an increased precipitation on islands is expected due to orographic processes. Snow primarily alters the surface albedo in ice covered situations, where snow albedo decrease from a winter value of 0.85 to a minimum of 0.64 in July. Values used are identical with those used in Björk and Söderkvist (2002) based on Maykut (1982). Snow albedo is thus always higher than the thickness dependant bare ice albedo in the range 0.2–0.6 (Björk and Söderkvist, 2002).

Both the mean wind and the standard deviation are higher during winter. The values used are based on Børresen (1987). Values are 1955–1981 monthly means from Hind-cast model runs incorporating local met stations. Stronger wind forcing in the model increases vertical heat fluxes and increases turbulent entrainment into the mixed layer. The model ocean volume transport is prescribed as a boundary condition, and does not use the wind forcing in any way.

The annual mean transport to the southern Barents Sea is 3.2 Sv, and to the northern Barents Sea it is 2.0 Sv. The flow carries heat, and in the south the standard value of 73 TW compares to cooling the 3.2 Sv from 5.6 °C to 0.0 °C. The annual mean ocean heat transport is also varied over a wide range. This spans changes in inflow, or outflow, temperature of $\pm1\,^\circ$C ($\pm$13 TW), and volume transport of $\pm$1 Sv ($\pm$23 TW). These sensitivity runs (50 TW to 96 TW) are included in Sect. 4.1 and cover the relatively large uncertainties in the real inflow and outflow of heat.

The volume transport used as forcing is equal to the monthly variation of the Atlantic inflow (Table 1). The transported heat is evenly distributed vertically, reflecting the homogeneous layer of Atlantic water in the BSO (Ingvaldsen et al., 2004).

The freshwater forcing used is based on the large scale freshwater budget discussed in Sect. 2.3, and is mimicking the effect of transport on the vertical salinity distribution. The salt budget is closed, so the mean salinity remains constant, and a stable model mean state, without drift in salinity, is found.

The magnitude of the salt redistribution is scaled by the volume transport. The inflowing Atlantic Water has salinity close to 35.1 (Skagseth, 2008), and the exiting water has salinity 34.75 (Gammelsrød et al., 2009). Both the inflow and outflow thus add, or "leave behind", salt to the Barents Sea mean salinity close to 35.0. If this was the only salinity forcing applied the Barents Sea salinity would increase significantly by $\sim$1 in 10 years. The surface freshening applied is the sum of the precipitation-evaporation, the sea ice, and parts of the NCC, together balancing the 20 mSv removed by the through flow.

The use of constant atmospheric parameters in this setup means that no feed-backs involving the atmosphere will be discussed. This relieves us from uncertainties involving cloud cover and corresponding changes in long wave radiation, and allow us to test sensitivity in a straightforward manner.

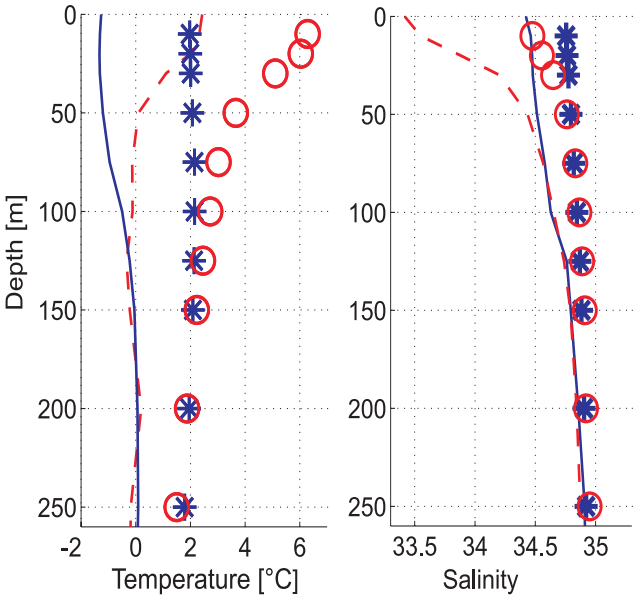

Fig. 4. Observed mean temperature and salinity in the Barents Sea. Summer data (June through September) are plotted in red, winter data (December through April) are plotted in blue. Data from "box south" are plotted using circles and asterisks, and for 'box north' using solid and dashed lines.

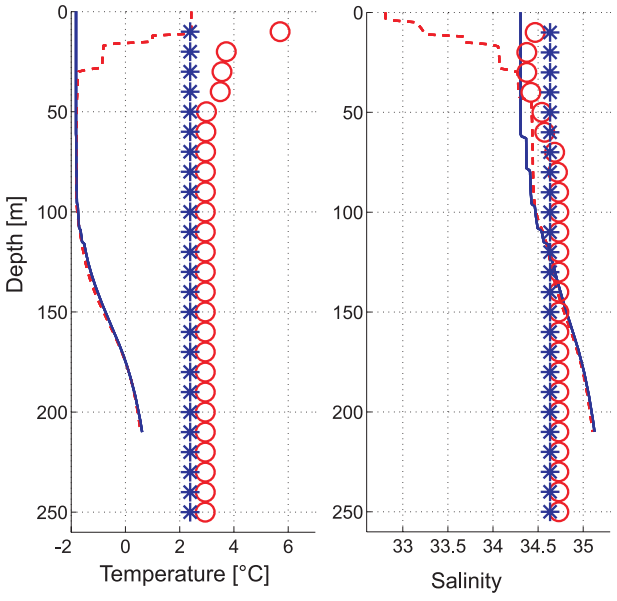

Fig. 5. Model profiles of Barents Sea temperature and salinity. Summer means (June–September) are plotted in red, winter (December–April) in blue. Results for box South are plotted using circles and asterisks, and for box North using solid and dashed lines.

3.2 Initialisation

Model runs were initiated in August using horizontally averaged profiles of temperature and salinity taken during summer. The averaged profiles are shown in Fig. 4, and are based on available stations in Nilsen et al. (2008) grouped into the "south box" and a "north box" indicated in Fig. 2. We will use the term "box" here, but the vertical dimension is sometimes maintained, so the term "column" could also have been used.

In the south box, data coverage is quite good, with all together 40 000 stations during winter and summer. In the north box there are 15 000 stations during summer, and 1700 stations during winter. The north box is best covered in its southern parts, particularly during winter. Possible spatial bias has been avoided by subdividing the region into smaller boxes and calculating individual mean profiles therefrom. Then these were averaged to produce overall mean profiles.

The south box receives nearly all of the ocean heat transport, and looses much of it to the atmosphere. The area over which this heat loss takes place is one of the key parameters of this model approach. The area used for the southern box is $900 \times 400\,\mathrm{km}^2$, which is ∼33% of the Barents Sea area. A total inflow of 3.2 Sv sets a flushing time (ocean volume divided by the inflow) for the southern box of about 1 year, using 253 m as mean depth. The remaining northern part is the largest area ($900 \times 810\,\mathrm{km}^2$). The area warmer than 0 °C in Fig. 2 is close to 50% of the Barents Sea, but sensitivity towards increasing the "south box" area is included in Sect. 4.2. To some extent we have "tuned" the area size to match the observed profiles, given the forcing discussed in Sect. 3.1. The flushing time for the northern box is about 2.5 years, using 210 m as mean depth and a total inflow of 2 Sv.

3.3 Southern Barents Sea results – south box

Summer temperature observations (Fig. 4) show a warm surface layer. Surface temperatures may reach 5–8 °C, and there are no other temperature maxima's below the surface. Downwards there is a gradual decrease to a thick homogeneous lower layer at 2–3 °C. Figure 5 shows that the 1DICE model is able to reproduce the main features of an annual cycle. The surface summer warming is close to observations, and a colder homogeneous water column is established in winter.

In summer the warm surface layer is also fresh, and salinities are usually around 34.5. The surface freshening is difficult to reproduce in the same way as the surface summer warming. This reflects uncertainties in surface freshwater balance (rain and transported freshwater in the surface layer), as discussed in Sect. 2.3. The applied salt redistribution works, but only in an approximate way. The freshwater balance is actually quite delicate. The model salinity also becomes homogeneous in winter, whereas the observations from "south box" indicate that it remains slightly stratified in salt.

The area used for the south box observed profiles is the area with higher mean winter surface temperatures than 0 °C in Fig. 2. The area warmer than 0 °C has changed over the last decades, and the sensitivity to changes in area of the south box, from the 1970's until today, is included in Sect. 4.4.

The summer temperature profiles used for validation (Fig. 4) are averages from 1 June to 30 September. The model profiles evolves, of course, throughout this period, and it is clear that observations are not evenly distributed in time. For instance, many of the observations are taken in August. Likewise for the winter period 1 December to 30 April, where many of the cruises are conducted in March and April. The observed "south box" winter mean temperature, both horizontally and vertically averaged, is 2.82 °C. The similar model mean temperature decreases from 3.22 °C in December to 1.7 °C in April (Fig. 7).

The annual cycle in temperature is thus in good agreement with observations, given the significant temporal and spatial variability of the observations, and the forcing. A perfect match between the average observed profiles and the model profiles is not expected. The maximum observed monthly summer mixed layer temperature of 6.35 °C is a good illustration, the model value is a little colder, 5.7 °C (Fig. 5). In general the 1DICE model is capable of reproducing the major features of the observed annual hydrographic changes in the southern box. Surface heat loss is given in Table 2, and discussed in Sect. 3.5.

3.4 Northern Barents Sea results – north box

The northern area is modelled using the same surface forcing as in the south. The observed northern profiles (Fig. 4) are used as initialisation, with a mean depth of 210 m. The ocean volume transport used is 2.0 Sv (Fig. 1), with a small heat transport of 2.0 TW. This ocean heat transport compares to the 2.0 Sv entering at 0.25 °C, and exiting at 0.0 °C. Results are not sensitive to a small increase of this heat, as long as it is below ∼5 TW. Using zero ocean heat transport, the northern box starts to drift towards a state where the entire column is at the freezing point during winter. Results do not depend on initialisation and a stable annual cycle is usually entered after three model years.

Figure 5 shows that a very different water column develops in the north, compared to the one in the southern Barents Sea. The annual cycle is confined to the mixed layer, and shows a shallow heated mixed layer in summer. Summer salinity of this mixed layer is as low as 33, caused by significant sea ice melt. From 50 to 100 m the column is at the freezing point, with an increasing salinity. This is similar to the cold halocline found over large areas of the Arctic Ocean (Rudels et al., 1996; Björk et al., 2002).

The summer surface-warming is close to observations, about 2 °C (Figs. 4 and 5). The model winter mixed layer temperature is at the freezing point (−1.8 °C), and the observations are around −1.0 °C. Winter observations tend to be taken quite late in the winter (March–April), when the sun has returned, and the sea ice starts to melt and open up. Until March most of the "North" area (Fig. 2) is 90% covered by sea ice (Budgell, 2005). It is therefore quite likely that the model winter mean (December–April) better reflects the real mean temperature than the observations taken mostly in late winter.

In the lower 100 m temperatures increases above 0 °C, similar to the Atlantic layer residing below the cold upper layer in the Eurasian basin. At the bottom salinity increases slightly above 35.0, and the column is so stable that there is no deep convection during winter.

Since the upper layer temperature in the model stabilizes below 0 °C, the northern box has a negative heat content referenced to this temperature. This means that the surface fluxes of this area drive the ocean column towards a state that will be a heat sink using 0.0 °C as a reference temperature, consistent with the estimated net heat transport from the Arctic Ocean to the Barents Sea (Gammelsrød et al., 2009).

Model salinity decreases slightly more than suggested by observations (Fig. 4) in the upper part of the column. Salinities also increase more in the deeper layers (Fig. 5). This increase at the bottom is caused by the salt redistribution resembling the transported contribution, and not salt rejected by sea ice growth. Winter sea ice growth is close to 1 m, but this ice melts again each summer predominantly due to the surface fluxes. The salt released during ice growth is counteracting the other freshwater sources in the top layer, and helps to homogenize the top 60 m during winter.

The model salinity in the deep increases above 35 as there is nothing in the model that counter-acts the transport of salt in the deep layer. This discrepancy may be caused by a number of factors. The salt redistribution applied here assumes a salinity of 34.75 for the 2.0 Sv exiting in BSX (Gammelsrød et al., 2009). There are probably additional salt fluxes connected to the sea ice that are not resolved by the model. Firstly, salt release from ice growth on shallow depth produces high salinity shelf water $S_w > 34.8$ that escapes close to bottom. Secondly, some of the sea ice freshwater imported from the Arctic Ocean probably leaves in the coastal current along the eastern shores of the Svalbard Islands. Thirdly, observations are quite scarce in the north, and high-salinity bottom water may largely have escaped sampling. These effects are all more pronounced in the northern box than in the south because of the sea ice growth, the stable column, and the lack of deep convection during winter.

3.5 Barents Sea surface heat loss

The Barents Sea has now been divided in two boxes. The south box gets all the ocean heat, the northern box only receives significant heat at the surface. The two averaged water columns are largely in line with the observed mean profiles

Table 2. Mean annual surface heat fluxes for the Barents Sea in TW. The 1-D total is our best estimate for the total Barents Sea. The "north box" contribution is quite small, and the major heat loss occurs in the "south box". The eight sensitivity runs are included at the bottom of the table, and are all performed over the "south box" area.

Heat flux	Total	Shortwave	Long wave	Sensible	Latent
Simonsen and Haugan	−135.2	69.9	−54.9	−85.0	−65.2
Zhang and Zhang	−39.3	78.1	−37.2	−17.4	−20.2
1-D total	−71.0	51.7	−45.2	−35.2	−42.3
north box	−3.8	25.7	−22.7	3.7	−10.5
south box (73 TW)	−67.2	26.0	−22.5	−38.9	−31.8
Morewater (+1 Sv, or 96 TW)	−94.6	26.4	−26.0	−53.0	−42.0
Lesswater (−1 Sv, or 50 TW)	−41.3	25.1	−19.0	−25.3	−22.1
Warmwater (+1 °C, or 86 TW)	−82.5	26.3	−24.5	−46.8	−37.6
Coldwater (−1 °C, or 60 TW)	−51.3	25.6	−20.4	−30.5	−25.9
Warm Air	−73.2	26.3	−25.6	−39.3	−34.7
Cold Air	−63.2	23.7	−11.3	−50.9	−24.7
Larger area (40%)	−51.6	25.5	−20.4	−30.7	−26.0
Largest area (50%)	−38.4	25.0	−18.6	−23.7	−21.1

from the boxes, confirming that this simple division is meaningful.

The transported 73 TW of ocean heat arriving in the BSO is lost to the atmosphere before reaching the northern box. But there is additional heat arriving as short wave radiation during summer. The annual mean model solar heating is 26 TW for the southern box, and 33 TW for the northern box. The two boxes receives the same solar radiation per m^2 (Table 1), but the total energy input is larger in the northern box because of its larger area. The difference in area is compensated by difference in sea ice cover, creating a solar input to the boxes of similar magnitude.

For the northern box also the sensible heat flux is positive into the ocean during summer, caused by air temperatures of 2–3 °C above the colder surface water. As mentioned earlier, the meteorological stations from the northern Barents Sea revealed air temperatures 2–3 °C lower than the mean forcing applied here during summer, indicating that the sensible heat flux might in reality be close to zero. Net long wave and latent heat fluxes are always negative both in the north and south. In the north the surface fluxes are close to being in balance, so the mean total heat flux is −3.8 TW. Given that the annual cycle varies between a loss of 80 TW and a gain of 120 TW (not shown), −3.8 TW is effectively zero. This means that nearly all of the ocean heat transport must be given up to the atmosphere over the southern 33% of the Barents Sea area.

The model average heat loss from the southern Barents Sea is 67 TW as shown in Fig. 6. This is 6 TW less than the ocean heat transport, and indicates a slow warming. This is confirmed in model profiles, where the mean temperature increases from 3.36 °C at initialisation, to 3.51 °C in year 6, but the difference is too small to be visible in Fig. 7. As noted in Sect. 2.2 have substantial year to year fluctuations occurred in the Atlantic heat transport, ranging from 30 to 60 TW.

The net heat loss from the south is partitioned into long wave, sensible, and latent heat fluxes (Fig. 6). Long wave radiation has a mean loss of 23 TW. There is 32 TW of latent heat loss, and 39 TW of sensible heat loss (Table 2). The annual cycle is smaller in the south than in the north, caused by the smaller area. The maximum net heat gain is 26 TW during summer. All three heat loss contributions peak during winter when there is no solar heating, causing the maximum heat loss of 150 TW. There are some days with a very thin ice cover during the winter. This ice quickly melts again as the oceanic heat is mixed upwards. The small portions of sea ice created by 1DICE lowers the heat fluxes during late winter, causing the reduced loss from ∼150 TW to ∼100 TW in December in Fig. 6.

The different heat fluxes are summarized in Table 2. The total heat loss from the two Barents Sea boxes used in the 1-D model add up to 71 TW, close to the transported 73 TW of heat by the ocean. The agreement is superficial in the way that the 73 TW was added to the southern box, but the northern box is demanding ∼3 TW totally on its own. The southern box reaches a close to stable state with the heat loss of 67.2 TW.

4 Discussion

The transported ocean heat to the Barents Sea is lost as long wave radiation, as well as latent and sensible heat fluxes. The simplified picture of the Barents Sea as two boxes is largely consistent with the earlier estimates of Simonsen and Haugan (1996) and Zhang and Zhang (2001). For all components

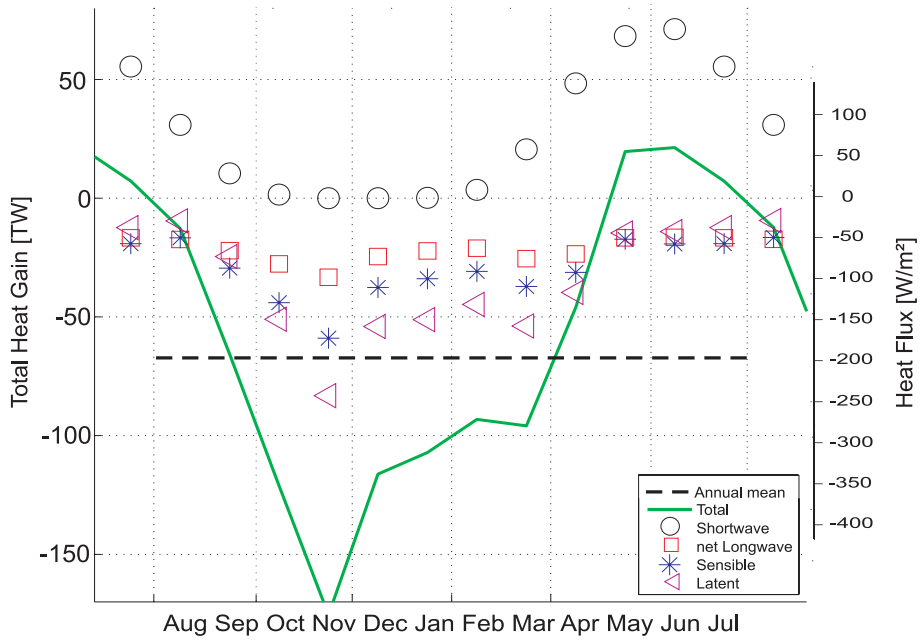

Fig. 6. Model heat gain for the southern Barents Sea. Values are plotted in tera Watt (1 TW=10^{12} W) for model year 5. The overall total heat gain is −67 TW, indicating a heat loss comparable to the ocean transport (black horizontal line). During summer the total heat gain is positive, peaking at 26 TW. The extra axis to the right is added to aid comparison with other surface flux estimates.

in Table 2 the 1-D results presented here are found between these earlier estimates.

In 1DICE the two largest contributions to the heat flux, the incoming short wave and the outgoing long wave, nearly cancel in the annual mean (Table 2). Such a balance is not found by Simonsen and Haugan (1996) and Zhang and Zhang (2001). Sensible and latent heat losses are significantly smaller than Simonsen and Haugan (1996), but larger than Zhang and Zhang (2001). In the northern box sensible heat fluxes do not contribute to the ocean heat loss. Our results show infact a small warming of the ocean, caused by the surface waters being close to freezing much of the year. The observed air temperature from the northern Barents Sea is of course lower than the mean air temperature for the whole sea, so this ocean warming may be an artifact of the 1-D approach. The monthly mean forcing is applied repeatedly for all years, and usually a stable situation is established during 3 years, as illustrated in Fig. 7.

We have not conducted sensitivity experiments for changes in the boundary conditions for freshwater transport. The estimates for freshwater transport are not as good as for heat transport, as fresh water tend to flow along the coasts. Significant unknown contributions may exist, especially around Svalbard and Franz Josef land.

4.1 Ocean heat transport variability

The ocean heat transport to the Barents Sea has varied during the last 10 years (Skagseth et al., 2008). In order to explore

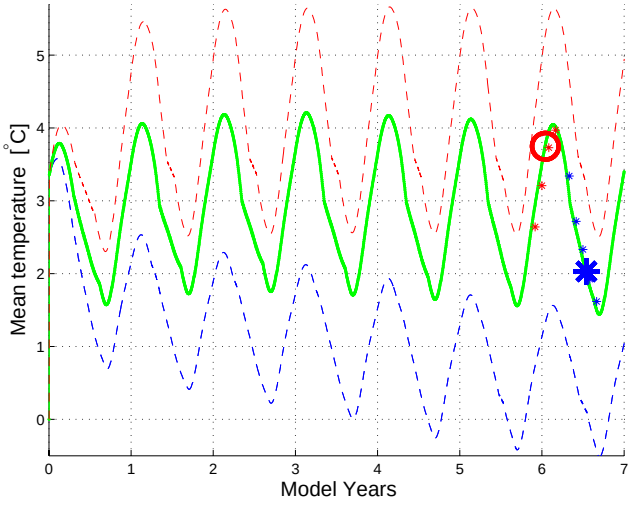

Fig. 7. Depth averaged model temperature of the southern Barents Sea. Results using the deduced mean ocean heat transport of 73 TW are shown by a green solid line. Individual months during year 6 are plotted for summer (June–September) as red asterisks, and winter (December–April) as blue. The observed winter mean (large blue asterisk) and summer mean (large red circle) is also plotted in year 6. Results using a 1 Sv decreased ("Lesswater" run, dashed blue line, 50 TW) and a 1 Sv increased ocean heat transport ("Morewater" run, red dash-dotted line, 96 TW) are also shown.

this dependence further the transport was varied around the mean state of 3.2 Sv and 73 TW used in the "south box" run.

Figure 7 shows how the depth-averaged temperature varies through the 6 first years in the "south box" run described in Sect. 3.3. Note that the same initial ocean column will be used for all sensitivity runs. Usually 1DICE also settles into a new stable annual cycle after about 3 years, comparable to the Barents Sea flushing time of 1–2.5 years. The observed winter mean value of 2.82 °C is found in the middle of the model results through the winter. The winter temperature is quite homogeneous, and is therefore a good indicator of available heat (Fig. 4).

Four runs are presented in Table 2 varying the ocean heat transport in different ways: "Morewater", "Lesswater", "Warmwater", and "Coldwater". As mentioned in Sect. 2.2 fluctuation in volume flux has governed ocean heat transport variability the last 10 years. In "Morewater" the monthly mean ocean volume transport (Table 1) has been increased with 1 Sv for all months through the year, giving an annual mean of 4.2 Sv. This creates an ocean heat transport of 96 TW. In the same manner "Lesswater" has an annual mean ocean transport of 2.2 Sv, and a heat transport of 50 TW.

In the "Morewater" run the 1 Sv increased ocean heat transport (96 TW) produces a warmer winter column as expected. Figure 7 shows that the summer maximum mean temperature reaches above 5 °C the second model summer. After model year 2 a new stable annual cycle is established, and mean surface fluxes are given in Table 2. The change is significant but moderate, and the warming during summer is larger than during winter. The annual cycle is increased in magnitude with 0.75 °C as shown in Fig. 7.

With an ocean heat transport lowered by 1 Sv (to 50 TW) in the "Lesswater" run, the Barents Sea water column cools by ∼2 °C (Fig. 7). The response is more continuous than for the "Morewater" run, and a gradual cooling appears throughout the 10 model years. After 6 years the winter mean temperature reaches 0 °C in winter. The accompanying heat fluxes are included in Table 2. Summer temperatures also cool down in the deep, but the solar radiation still warm up the surface layer to around 4 °C (not shown).

The effect of removing 1 Sv in the "Lesswater" run is thus larger than adding 1 Sv in the "Morewater" run. This probably reflects both the importance of the ocean heat transport to the Barents Sea and that the atmospheric heat loss has a damping effect on fluctuations in the transported heat. If the heat transport decrease, the model immediately starts to cool down. The real ocean would probably respond in this way too, but in addition change the area of the box. On the other hand, when the heat transport increase, the heat loss during winter will also increase. Figure 7 shows that the amplitude of the annual temperature cycle increases with increasing ocean transport, and that the summer temperatures changes the most. The heat transport driven changes are thus dampened more during the cold season than during the warm season.

In the "Warmwater" run the inflow temperature has been increased by 1 °C, this increases the ocean heat transport from 73 TW to 86 TW. This heat transport is mid way between the "south box" and "Morewater" runs, and the total model heat loss becomes 82.5 TW. The other surface fluxes are included in Table 2. The effect on mean winter and summer temperatures is plotted in Fig. 8, together with the other sensitivity runs. The variation in temperature are clearly damped in the Barents Sea. The increase of 1 °C at the boundary results in an increase of ∼0.75 °C in the mean. Such a damping of the oceanic signals in the Barents Sea has earlier been observed by Schauer et al. (2002) and Ingvaldsen and Gjøsæter (2010). Even though the effect of increasing the temperature with 1 °C is smaller than the effect of increasing the volume flux by 1 Sv, it gives a highly significant contribution (Fig. 8). While the volume flux has a strong variation on inter-annual time scales (Ingvaldsen et al., 2004), the inflowing temperature shows long-term trends and has increased by more than a degree since the late 1970s (Skagseth et al., 2008). Thus variability in the inflow temperature is likely to be highly important on longer time scales.

The effect of decreasing inflow temperature by 1 °C is shown in the "Coldwater" run, lowering the ocean heat transport to 60 TW (Fig. 8). Again we find a damping in the Barents Sea, the mean winter and summer temperatures are lowered by less than the 1 °C decrease of the inflow. As in the "Lesswater" run the damping is stronger during winter, than during summer. The mean surface fluxes are tabulated in Table 2.

Using a smaller transport than 50 TW of heat creates some unexpected results (not shown). An ocean heat transport of 40 TW produces a surface heat loss around 12.5 TW, much smaller than the added heat. This means that the Barents Sea water column heats up with about 27 TW, producing a mean temperature around 5 °C in 4 years. In this situation the cooling during winter is not strong enough to erode the fresher surface mixed layer established during summer. Consequently, there is no homogeneously mixed water column during winter, and the warm water remains isolated from the cold atmosphere. The winter convection and cooling reach about 50 m depth, so temperature remains around 0 °C in the top 50 m. After four model years results become unrealistic and points to the limitation of the 1-D model and the added salt redistribution. Despite the limitations of the 1-D approach, the results indicate a lower limit on heat transport to the Barents Sea beyond which a transition into a new steady state would start. This new steady state has the same qualitative properties as the Arctic Ocean, with a warmer Atlantic layer below a colder, and stable, upper layer.

4.2 Changes in cooling area

The main balance in the 1DICE model is between the ocean heat transport and the area available for cooling this water.

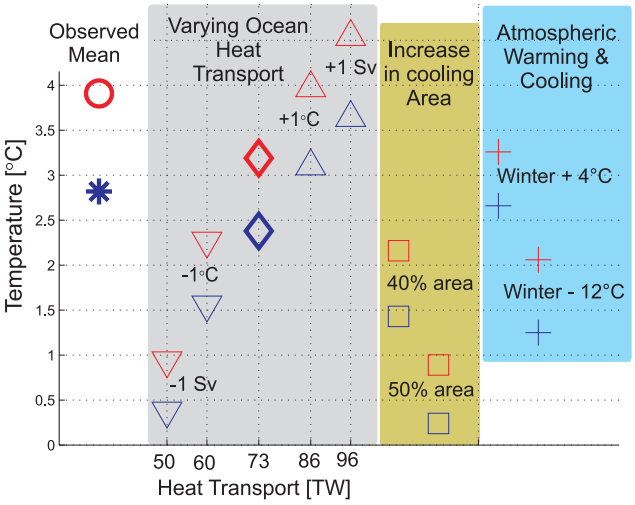

Fig. 8. Averaged model winter (blue) and summer (red) temperatures of the southern Barents Sea from the different sensitivity tests. Model runs are described in the text (Table 2). Observationally based summer (red circle) and winter (blue asterisk's) are found to the left, and the standard run "south box" values are plotted as diamonds.

Increasing the size of the area in "box south" leads to a larger heat loss.

The northern and southern boxes are driven by exactly the same monthly mean forcing, and the model runs therefore support a few new balances within the Barents Sea. The northern part gets little ocean heat transport and naturally enters a state that produces sea ice every winter. It also has an upper water column at the freezing point, and a small ocean to air heat loss (∼3 TW). Such an ocean column covers a relatively large part of the Barents Sea, in our model it is about 66% of the area.

The southern box, driven by exactly the same surface forcing, enters a totally different regime because of the transported ocean heat. The area used in this model, 33% of the Barents Sea, produces a fairly good agreement with the observed mean temperatures. The long-term mean area warmer than 0 °C during winter (Fig. 2) is however close to 50% of the Barents Sea. If a larger area is used for the southern box keeping the transported ocean heat at 73 TW, the temperatures in the box decrease. Two runs using an increased "box south" area to 40% and 50% of the Barents Sea, give decrease in mean temperature of 1.0 and 2.5 °C, respectively (Fig. 8).

The reduced temperature could indicate, for example, uncertainties of the extracted monthly forcing. They could also indicate limitations of the simple column model approach, or that the main heat loss actually takes place over an area significantly smaller than the 50%. The cooling area could be defined in many ways; water warmer than some limit, the position of Polar Front, or the ice free area. Regardless of the definition large changes in the cooling area occur regularly in the Barents Sea (e.g. Loeng, 1991; Vinje, 2001; Sorteberg and Kvingedal, 2006; Ådlandsvik, 2010). More important than finding the exact area corresponding to the mean situation, is finding how changes in the cooling area relates to changes in the ocean heat transport and how this affects the balance in the region.

Over the period 1997–2006 the volume flux in the BSO increased by 1 Sv and the inflow temperature increased by 1 °C (Skagseth et al., 2008). According to Fig. 8 this should cause the winter and summer mean temperature of the southern Barents Sea to increase significantly. The response for mean temperature towards variation in ocean heat transport is close to linear, and observations suggest adding the "Morewater" and "Warmwater" runs, i.e. a warming of around 2 °C. Such a large general warming has not been observed. However, a simultaneous increase in cooling area of 10–20% would reduce the temperature increase to 0.5–1.0 °C which is more in line with the observations.

4.3 Atmospheric warming and cooling

The Barents Sea region has experienced a significant atmospheric warming the last 10 years (Zhang et al., 2008). Winter observations from Bear Island (not shown) has increased from around −8 °C for the 1960–1990 period to around −2 °C for the 2005–2008 period. How much has this warming affected the Barents Sea? To investigate this, the mid winter air temperature was increased from −12 °C to −8 °C. For the other months the air temperature was increased by 1 °C (see air temperatures in Table 1).

For the ocean temperatures, the effects are small (Fig. 8). The winter mean temperature increases with 0.22 °C. The warmer air has other significant impacts, on the sea ice thickness in the northern Barents Sea, for example, but we let that issue rest.

In this study, mean air temperatures from the ERA 40 and NCEP reanalysis covering the entire Barents Sea were used. These air temperatures were found to be comparable to means from met stations in the southern Barents Sea. Our 1DICE model nevertheless reproduce a cold northern ocean, with small air-sea sensible and latent heat fluxes. The interannual variability in the air temperatures is large, and to evaluate the effect of decreased winter air temperatures, a sensitivity run was performed for the southern box using mean temperatures based on available meteorological stations in the Northern Barents Sea. These stations have a mid winter air temperature around −25 °C. The colder air increases the sensible heat loss, but also decreases latent heat loss (Table 2). The long wave radiation heat loss also decreases as a result of lower sea surface temperatures. The effect on the Barents Sea mean temperatures are modest; a cooling of 0.75–1.00 °C is small, considering the extremely cold air (Fig. 8).

These results indicate that air temperatures have a modest effect on the overall heat loss, especially compared to the cooling area.

4.4 Decadal variability

Hydrographic data back to the 1970's was assembled and used to produce the mean hydrographic climatology of the NISE data set (Nilsen et al., 2008). Our aim was originally to also present decadal estimates of the variability in the Barents Sea heat storage. Some sections are available on a regular basis back to 1980, like the one across the BSO (Furevik, 2001). The Russian Kola section is also available back to about 1910, and shows a multi-decadal signal similar to the Atlantic Multi decadal Oscillation (Skagseth et al., 2008). In general the profiles are not available evenly distributed in time and space, and we found that horizontally averaged temperatures over decadal time frames have questionable representativity.

The minimum annual mean temperature of the Atlantic layer in the BSO was 4.3 °C in 1978, and the maximum was 6.4 °C in 2006 (Skagseth et al., 2008). This range probably carries a general warming trend, and the normal decadal variability in temperature is around ±0.5 °C. In line with our findings above the deeper layers in the BSO have the larger variability, and the warming and cooling episodes of the 1980's are generally stronger at 400 m than they are closer to the surface (Furevik, 2001).

In the BSX there are also some indications of a warming since the 1970's (Ingvaldsen and Gjøsæter, 2010). The NISE data grouped into pentades (not shown) indicate a warming in the BSX of ∼0.5 °C from the mid 1970's to the mid 1990's. Our column model setup is forced with ocean transport data since 1997, when the mean temperature in the BSX has been close to 0 °C. A possible further warming above 0 °C of the outflow temperature in the model setup would produce a heat transport out of the Barents Sea. The magnitude of these changes is however well within the sensitivity test of decreasing ocean heat transport to the Barents Sea (Fig. 8). This is clearly an important issue that deserves further investigation when better data become available.

The observed decadal variability is around ±0.5 °C. This is a significantly smaller variability than one could expect based on the observed changes in inflow during the last decade. Figure 8 therefore indicates that the Barents Sea has responded to increasing ocean heat transport by increasing the area where the heat loss takes place.

5 Conclusions

An updated synthesis indicates that the ocean volume transport to the southern Barents Sea is 3.2 Sv. This flow carries 73 TW of heat, and removes the excess freshwater entering by rain, sea ice, and ∼18% of the Norwegian Coastal Current. The part transported by Atlantic Water is 50 TW of heat in 2.0 Sv of water.

Horizontally averaged profiles of temperature and salinity show that the Barents Sea may be qualitatively divided into two columns. The northern column is stratified in salinity, and has a surface layer close to the freezing point during winter. The southern column mixes deep down during winter and is re-stratified every summer by the solar heating.

A column model is used to reproduce these two regions of the Barents Sea. Average monthly forcing is applied, and usually a new stable state is established within 3–5 years. The surface summer warming and freshening takes place both in the northern and southern Barents Sea, while the deep convection in winter only appears in the south. Model results thus reproduce the mean summer and winter profiles of temperature in a good way, but the average salinity profiles are more sensitive to the freshwater forcing.

The heat transported to the southern Barents Sea is lost as sensible and latent heat fluxes. In this area short wave and long wave radiation nearly cancel over a year, with a small net ocean warming of 3 TW. A stable annual cycle in mean temperature with a minimum of 1.8 °C in late winter and a maximum of 4.1 °C in late summer is established in the south.

The northern Barents Sea receives little ocean heat, and ∼1 m of sea ice grows and melts every year. The annual mean total heat loss is around 4 TW in the north. The combined solar and long wave radiation has the same small positive contribution as in the south (3 TW), but in the north sensible and latent heat fluxes are also small.

The column model shows a close to linear relation between ocean heat transport and the mean temperature in the Barents Sea. For the southern Barents Sea an inflow warming of +1 °C, corresponding to an increased heat transport of 13 TW, would result in a ∼0.8 °C warming. The mean temperature also depends on the cooling area, and this increased ocean heat transport can be compensated by a 10% increase in the cooling area.

In recent years a northward shift of the Polar Front, a related northward shift of the winter ice edge, and an increased ocean heat transport has been observed. Our model approach reproduces the two mechanisms one by one, and can therefore explain their relative importance in nature. If this expansion in cooling area did not occur, the warming would have been much larger.

The Barents Sea is an effective and robust ocean cooler. The observed variability in volume and inflow temperature is large, but the variability in mean temperature, or stored heat, is low. Our results therefore indicate that the ocean heat transport modulates both the Barents Sea mean temperature, and the area over which cooling occurs. When the heat transport increases, the warm water spreads further into the sea, causing cooling over a larger area. This is consistent with a retreat of the sea ice cover as suggested by Sorteberg

and Kvingedal (2006), and a temperature that varies in phase over the southern Barents Sea (Ingvaldsen et al., 2003).

As a result, the water leaving the Barents Sea toward the Arctic Ocean has temperatures close to 0 °C. The northern Barents Sea does not contribute significantly to the cooling, but acts as a buffer into which the southern effective cooling area may expand.

Acknowledgements. This work was completed as a part of the Polar Climate and Heat Transport (Pocahontas) and the Bipolar Atlantic Thermohaline Circulation (BIAC) projects, both funded by the Research Council of Norway. The atmospheric forcing data was provided by Asgeir Sorteberg (Geophysical Institute, University of Bergen), but he was, unfortunately, to busy to join in at the writing stage. Thanks to Eva Falck for helpful language improvements, and to Bert Rudels, and two other anonymous reviewers, for important clarifications and good suggestions. The ocean temperature and salinity data were provided by: the Marine Research Institute, Iceland; Institute of Marine Research, Norway; the Faroese Fisheries Laboratory; the Arctic and Antarctic Research Institute, Russia, and Geophysical Institute, University of Bergen, Norway, through the NISE project. This is publication A237 from the Bjerknes Centre for Climate Research.

Edited by: S. Josey

References

Aagaard, K. and Carmack, E.: The role of Sea Ice and Other Fresh Water in the Arctic Circulation, J. Geophys. Res., 94, 14485–14489, 1989.

Ådlandsvik, B.: The Polar Front in the Barents Sea, in preparation, 2010.

Aksenov, Y., Bacon, S., Coward, A., and Nurser, A.: The North Atlantic inflow to the Arctic Ocean: High-resolution model study, J. Marine Syst., 79(1–2), 1–22, doi:10.1016/j.jmarsys.2009.05.003, 2010.

Årthun, M. and Schrum, C.: Ocean surface heat flux variability in the Barents Sea, J. Marine Syst., submitted, 2010.

Björk, G.: A One-Dimensional Time-Dependant Model for the Vertical Stratification of the Upper Arctic Ocean, J. Phys. Oceanogr., 19, 52–67, 1989.

Björk, G.: The relation between ice deformation, oceanic heat flux, and the ice thickness distribution in the Arctic Ocean, J. Geophys. Res., 102, 18689–18698, 1997.

Björk, G. and Söderkvist, J.: Dependence of the Arctic Ocean ice thickness distribution on the poleward energy flux in the atmosphere, J. Geophys. Res., 107(C10), 3173, doi:10.1029/2000JC000723, 2002.

Björk, G., Söderkvist, J., Winsor, P., Nikolopoulus, A., and Steele, M.: Return of the cold halocline layer to the Amundsen Basin in the Arctic Ocean: Implications for sea ice mass balance, Geophys. Res. Lett., 29, 1513, doi:10.1029/2001GL014157, 2002.

Blindheim, J.: Cascading of Barents Sea bottom water into the Norwegian Sea, Rapports et Proces-verbaux Réunions Conceil permanent International pour l'Exploration de la Mer, 226, 49–58, 1989.

Børresen, J. A.: Wind Atlas for the North Sea and the Norwegian Sea, Tech. rep., The Norwegian Meteorological Institute, Norwegian University Press, ISBN 82-00-35276-5, 1987.

Budgell, P.: Numerical simulation of ice–ocean variability in the Barents Sea region Towards dynamical downscaling, Ocean Dynam., 55(3–4), 370–387, doi:10.1007/s10236-005-0008-3, 2005.

Dankers, R. and Middelkoop, H.: River discharge and freshwater runoff to the Barents Sea under present and future climate conditions, Climate Change, 87, 131–153, doi:10.1007/s10584-007-9349-x, 2008.

Dickson, R., Osborn, T., Hurrell, J., Meincke, J., Blindheim, J., Ådlandsvik, B., Vinje, T., Alekseev, G., and Maslowski, W.: The Arctic Ocean Response to the North Atlantic Oscillation, J. Climate, 13, 2671–2696, 2000.

Dickson, R., Rudels, B., Dye, S., Karcher, M., Meincke, J., and Yashayaev, I.: Current estimates of freshwater flux through Arctic and subarctic seas, Prog. Oceanogr., 73, 210–230, 2007.

Drange, H., Gerdes, R., Gao, Y., Karcher, M., Kauker, F., and Bentsen, M.: Ocean general circulation modelling of the Nordic Seas, in: The Nordic Seas, An Integrated Perspective, edited by: Drange, H., Dokken, T., Furevik, T., Gerdes, R., and Berger, W., American Geophysical Union, Washington DC, 199–220, 2005.

Eisenman, I., Untersteiner, N., and Wettlaufer, J.: On the reliability of simulated Arctic sea ice in global climate models, Geophys. Res. Lett., 34, L10501, doi:10.1029/2007GL029914, 2007.

Furevik, T.: Annual and interannual variability of Atlantic Water temperatures in the Norwegian Seas: 1980–1996, Deep-Sea Res., 48, 383–404, 2001.

Gammelsrød, T., Leikvin, Ø., Lien, V., Budgell, W., Loeng, H., and Maslowski, W.: Mass and heat transports in the NE Barents Sea: Observations and models, J. Marine Syst., 75, 56–69, doi:10.1016/j..marsys.2008.07.010, 2009.

Gerdes, R., Karcher, M., Kauker, F., and Schauer, U.: Causes and development of repeated Arctic Ocean warming events, Geophys. Res. Lett., 30, 1980, doi:doi:10.1029/2003GL018080, 2003.

Harms, I., Schrum, C., and Hatten, K.: Numerical sensitivity studies on the variability of climate-relevant processes in the Barents Sea, J. Geophys. Res., 110, C06002, doi:10.1029/2004JC002559, 2005.

Ingvaldsen, R. and Gjøsæter, H.: Impact of climate variability, stock size and age composition on the spatial distribution of Barents Sea capelin, submitted, 2010.

Ingvaldsen, R., Loeng, H., Ottersen, G., and Ådlandsvik, B.: Climate variability in the Barents Sea during the 20th century with focus on the 1990s, ICES Marine Science Symposia, 219, 160–168, 2003.

Ingvaldsen, R., Asplin, L., and Loeng, H.: The seasonal cycle in the Atlantic transport to the Barents Sea during the years 1997–2001, Cont. Shelf Res., 24, 1015–1032, 2004.

Karcher, M., Kulakov, M., Pivovarov, S., Schauer, U., Kauker, F., and Schlitzer, R.: Atlantic Water flow to the Kara Sea: Comparing model results with observations, in: Proceeding in Marine Science, Siberian River Run-off in the Kara Sea: Characterisation, Quantification, Variability and Environmental Significance, edited by: R. Stein, R., Fahl, K., Futterer, D., and Galimov, E., 47–69, 2003.

Loeng, H.: Features of the physical oceanographic conditions of the Barents Sea, Polar Res, 10, 5–18, 1991.

Loeng, H., Ozhigin, V., and Ådlandsvik, B.: Water fluxes through the Barents Sea, ICES J. Marine Sci., 54, 310–317, 1997.

Maslowski, W., Marble, D., Walczowski, W., Schauer, U., Clement, J. L., and Semtner, A. J.: On climatological mass, heat, and salt transports through the Barents Sea and Fram Strait from a pan-Arctic ice-ocean model simulation, J. Geophys. Res., 109, C03032, doi:10.1029/2001JC001039, 2004.

Maykut, G.: Large scale heat exchange and ice production in the central Arctic, J. Geophys. Res., 87, 7971–7984, 1982.

Montgomery, R.: Comments on seasonal variability of Florida Current - Niiler and Richardson, J. Marine Res., 32, 533–534, 1974.

Mosby, H.: Water, salt and heat balance of the North Polar Sea and the of the Norwegian Sea, Geofysiske Publikasjoner (Geophysica Norvegica), 24, 289–313, 1962.

Nilsen, J. E. Ø., Hátún, H., Mork, K. A., and Valdimarsson, H.: The NISE Dataset, Technical Report 08-01, Faroese Fisheries Laboratory, Box 3051, Tórshavn, Faroe Islands, 2008.

O'Dwyer, J., Kasajima, Y., and Nøst, O.: North Atlantic Water in the Barents Sea Opening, 1997 to 1999, Polar Res., 2, 209–216, 2001.

Pavlov, V., Pavlova, O., and Korsnes, R.: Sea ice fluxes and drift trajectories from potential pollution sources, computed with a statistical sea ice model of the Arctic Ocean, J. Marine Syst., 48, 133–157, 2004.

Rudels, B., Anderson, L., and Jones, E.: Formation and evolution of the surface mixed layer and halocline of the Arctic Ocean, J. Geophys. Res., 101, 8807–8821, 1996.

Sandø, A. B., Nilsen, J. E. Ø., Gao, Y., and Lohmann, K.: The importance of Heat Transports and local Air–Sea Heat Fluxes to the Barents Sea Climate Variability, J. Geophys. Res., submitted, 2010.

Schauer, U., Loeng, H., Rudels, B., Ozhigin, V., and Dieck, W.: Atlantic Water flow through the Barents and Kara Seas, Deep-Sea Res I, 49, 2281–2298, 2002.

Schauer, U., Beszczynska-Möller, A., Walczowski, W., Fahrbach, E., Piechura, J., and Hansen, E.: Variation of Measured Heat Flow Through the Fram Strait Between 1997 and 2006, in: Arctic - Subarctic Ocean Fluxes, edited by Dickson, R., Meincke, J., and Rhines, P., Springer Verlag, 65–85, 2008.

Serreze, M., Barrett, A., Slater, A., Woodgate, R. A., Aagaard, K., Lammers, R. B., Steele, M., and Moritz, R.: The large-scale freshwater cycle of the Arctic, J. Geophys. Res., 111, C11010, doi:10.1029/2005JC003424, 2006.

Serreze, M., Barrett, A., Slater, A., Steele, M., Zhang, J., and Trenberth, K.: The large-scale energy budget of the Arctic, J. Geophys. Res., 112, D11122, doi:10.1029/2006JD008230, 2007.

Simonsen, K. and Haugan, P. M.: Heat budgets for the Arctic Mediterranean and sea surface heat flux parameterizations for the Nordic Seas, J. Geophys. Res., 101, 6553–6576, 1996.

Skagseth, Ø.: Recirculation of Atlantic Water in the western Barents Sea, Geophys. Res. Lett., 35, L11606, doi:10.1029/2008GL033785, 2008.

Skagseth, Ø., Furevik, T., Ingvaldsen, R., Loeng, H., Mork, K., Orvik, K., and Ozhigin, V.: Volume and heat transport to the Arctic Ocean via the Norwegian and Barents Seas, in: Arctic – Subarctic Ocean Fluxes, edited by: Dickson, R., Meincke, J., and Rhines, P., Springer Verlag, 45–64, 2008.

Skagseth, Ø., Drinkwater, K., and Terrile, E.: Wind-induced transport of the Norwegian Coastal Current in the Barents Sea, J. Geophys. Res., submitted, 2010.

Sorteberg, A. and Kvingedal, B.: Atmospheric Forcing on the Barents Sea Winter Ice Extent, J. Climate, 19, 4772–4784, 2006.

Vinje, T.: Anomalies and trends of sea-ice extent and atmospheric circulation in the Nordic Seas during the period 1865–1998, J. Climate, 14, 255–267, 2001.

Walsh, J., Kattsov, V., Portis, D., and Meleshko, V.: Arctic Precipitation and Evaporation: Model Results and Observatinal Estimates, J. Climate, 11, 72–87, 1998.

Zhang, X. and Zhang, J.: Heat and freshwater budgets and pathways in the Arctic Mediterranean in a coupled Ocean/Sea-ice Model, J. Oceanogr., 57, 207–234, 2001.

Zhang, X., Sorteberg, A., Zhang, J., Gerdes, R., and Comiso, J.: Recent radical shifts of atmospheric circulations and rapid changes in Arctic climate system, Geophys. Res. Lett., 35, L22701, doi:10.1029/2008GL035607, 2008.